Water Resources Research

RESEARCH ARTICLE
10.1029/2019WR026225

Impact of Flow Alteration and Temperature Variability on Hyporheic Exchange

Liwen Wu[1,2,3], **Jesus D. Gomez-Velez**[3,4], **Stefan Krause**[5,6], **Tanu Singh**[5], **Anders Wörman**[7], **and Jörg Lewandowski**[1,2]

[1]Department of Ecohydrology, Leibniz-Institute of Freshwater Ecology and Inland Fisheries, Berlin, Germany, [2]Geography Department, Humboldt-University, Berlin, Germany, [3]Department of Civil and Environmental Engineering, Vanderbilt University, Nashville, TN, USA, [4]Department of Earth and Environmental Sciences, Vanderbilt University, Nashville, TN, USA, [5]School of Geography, Earth and Environmental Sciences, University of Birmingham, Birmingham, UK, [6]LEHNA-Laboratory of Ecology of Natural and Man-Impacted Hydrosystems, University Claude Bernard Lyon 1, Lyon, France, [7]Division of River Engineering, Royal Institute of Technology, Stockholm, Sweden

Key Points:
- Typical hydrological regimes corresponding to different levels of flow alteration are identified
- Including temporal variability of river temperature results in substantial differences in hyporheic exchange characteristics
- Alteration of river flow reduces the potential of hyporheic zones to act as a temperature buffer

Supporting Information:
- Supporting Information S1
- Figure S1
- Figure S2
- Figure S3
- Figure S4
- Figure S5
- Figure S6

Correspondence to:
L. Wu,
liwen.wu@igb-berlin.de

Citation:
Wu, L., Gomez-Velez, J. D., Krause, S., Singh, T., Worman, A., & Lewandowski, J. (2020). Impact of flow alteration and temperature variability on hyporheic exchange. *Water Resources Research*, *56*, e2019WR026225. https://doi.org/10.1029/2019WR026225

Received 24 AUG 2019
Accepted 19 FEB 2020
Accepted article online 20 FEB 2020

Abstract Coupled groundwater flow and heat transport within hyporheic zones extensively affect water, energy, and solute exchange with surrounding sediments. The local and cumulative implications of this tightly coupled process strongly depend on characteristics of drivers (i.e., discharge and temperature of the water column) and modulators (i.e., hydraulic and thermal properties of the sediment). With this in mind, we perform a systematic numerical analysis of hyporheic responses to understand how the temporal variability of river discharge and temperature affect flow and heat transport within hyporheic zones. We identify typical time series of river discharge and temperature from gauging stations along the headwater region of Mississippi River Basin, which are characterized by different degrees of flow alteration, to drive a physics-based model of the hyporheic exchange process. Our modeling results indicate that coupled groundwater flow and heat transport significantly affects the dynamic response of hyporheic zones, resulting in substantial differences in exchange rates and characteristic time scales of hyporheic exchange processes. We also find that the hyporheic zone dampens river temperature fluctuations increasingly with higher frequency of temperature fluctuations. This dampening effect depends on the system transport time scale and characteristics of river discharge and temperature variability. Furthermore, our results reveal that the flow alteration reduces the potential of hyporheic zones to act as a temperature buffer and hinders denitrification within hyporheic zones. These results have significant implications for understanding the drivers of local variability in hyporheic exchange and the implications for the development of thermal refugia and ecosystem functioning in hyporheic zones.

1. Introduction

Rivers continually exchange water, energy, solutes, and microorganisms with their surrounding sediments, creating subsurface areas that contain sets of flow lines that begin and end at the sediment-water interface. These areas are called hyporheic zones (Gooseff, 2010; Harvey et al., 1996). Hyporheic zones are characterized by strong physical and chemical gradients that modulate fluvial biological diversity and geochemical cycling (see Boano et al., 2014; Lewandowski et al., 2019, and reference therein). The hyporheic zone's spatiotemporal variability depends on pressure gradients at the sediment-water interface, which change dynamically with river discharge, and hydraulic properties of the porous media. For example, hydraulic conductivity is a function of changing flow temperature (Bear, 1972), which makes it an important variable determining hyporheic exchange processes. Capturing the effects of temporal variability in channel discharge and temperature in a wide range of scenarios requires a fully coupled modeling approach that represents both flow of water and transport of energy.

Hyporheic exchange fluxes demonstrate a dynamic response to time-varying discharge conditions. Increasing hydraulic gradients drive more surface water through the sediment, enlarging the spatial extent of the hyporheic zone (Schmadel et al., 2016; Singh et al., 2019). However, this general trend can be modulated substantially by regional groundwater flow conditions (Lewandowski et al., 2009; Malzone et al., 2016; Marzadri et al., 2016; Trauth & Fleckenstein, 2017; Wu et al., 2018), local geomorphological settings (Boano et al., 2013; Gomez-Velez et al., 2017; Tonina & Buffington, 2011; Ward et al., 2017), and heterogeneity in

streambed hydraulic conductivities (Cardenas et al., 2004; Gomez-Velez et al., 2014; Kalbus et al., 2009; Sawyer & Cardenas, 2009). Local groundwater interactions (i.e., gaining and losing) result in hyporheic zone contraction due to less surface water penetrating through the sediment (Cardenas & Wilson, 2007b; Wu et al., 2018). Additionally, the geomorphological setting can modify the transient hydraulic head distribution at the sediment-water interface. High aspect ratios (the ratio between the bedform amplitude and wavelength) and steep channel slopes often contribute to a fast hyporheic responses to changing discharge (Malzone et al., 2016; Singh et al., 2019). Heterogeneity in physical sediment properties can alter hyporheic exchange flow paths and residence time distributions (Gomez-Velez et al., 2014). So far, the analysis of dynamic responses of hyporheic exchange fluxes to changes in river discharge usually lacks a detailed consideration of river temperature impacts.

River temperature substantially affects the dynamic thermal responses of hyporheic system by a number of physical processes. At the atmosphere-river interface, energy is exchanged through solar or short-wave radiation, long-wave radiation, evaporative processes, and convective transfer due to temperature differences at this interface (Olden & Naiman, 2010; Poole & Berman, 2001). Heat exchanges at the sediment-water interface is controlled by heat conduction, advection, and thermal dispersion through groundwater inputs and hyporheic exchanges (Anderson, 2005). The rates of heat exchanges in hyporheic zones are affected by atmospheric boundary conditions, groundwater interactions, river discharges (Ferencz & Cardenas, 2017; Gerecht et al., 2011), topography, streambed geology, sediment properties (Caissie, 2006; Wörman et al., 2012), and anthropogenic activities such as flow regulations (Ward, 1985) and the presence of man-made in-stream structures (i.e., large woody debris and weirs) (Hester et al., 2009; Sawyer et al., 2012). These factors create a dynamic multiscale thermal mosaic across fluvial systems. Aquatic species use a diverse array of thermal habitats to meet their specific temperature requirements for survival, growth, and reproduction (Olden & Naiman, 2010). Temperature variability also extensively modifies the nutrient cycling and the spatial distribution of biogeochemical reaction hot spots in hyporheic zones (Song et al., 2018; Zheng & Cardenas, 2018). However, the temperature sensitivity of ecological and biogeochemical processes is often examined under oversimplified constant flow boundary conditions.

Natural flow regimes have been regulated and altered for different purposes serving important human needs, such as irrigation, energy production, water resources, and flood control (Abril et al., 2015; Weiskel et al., 2010). Flow alteration has substantial impacts on characteristic time scales for flow of water and transport of heat along river networks, including the magnitude of peak flows, duration of recession periods, and the amplitude of diel temperature oscillations (Olden & Naiman, 2010; Poole & Berman, 2001; Sawyer et al., 2009). Consequently, flow alteration has profound implications for hyporheic exchange across multiple scales, on local and regional ecosystem services and water quality. The interactions between surface water and groundwater further complicate heat transport due to variable degrees and time scales of temperature variations in both systems. Groundwater temperature fluctuates predominantly over longer seasonal scales while surface water temperatures often vary over multiple time scales, including event-based, diel, and seasonal fluctuations (Constantz, 1998; Constantz et al., 1994; Todd & Mays, 2005). The temperature dynamics in the hyporheic zone therefore closely depend on site-specific groundwater-surface water interactions. Understanding coupled responses of hyporheic zones to river flow and temperature variations becomes imperative to evaluate the impacts of flow alterations.

Previous research on dynamic hyporheic exchange focused predominantly on identifying the impact of individual drivers, such as river discharge or temperature (Figures 1a–1d or 1e–1g), but did not specifically account for the joint impacts of these two driving forces (Figure 1h). Hyporheic exchanges of flow and energy are highly temperature dependent. This is due to the temperature dependency of fluid density and viscosity which contributes to a varying hydraulic conductivity over time (Constantz et al., 1994; Ling & Dybbs, 1992; Ramirez & Saez, 1990). The thermally induced fluid viscosity variations can extensively modify the hyporheic flux (Cardenas & Wilson, 2007a) and consequently control biogeochemical activities. Nevertheless, most of the previous studies that couple the modeling of flow and heat exchange processes are either sequentially coupled and use precalculated flow fields as boundary conditions of the subsequent heat transport modeling (Hester et al., 2009; Marzadri et al., 2013) or couple heat and flow modeling by considering only steady discharge (Burkholder et al., 2008; Cardenas & Wilson, 2007a; Marzadri et al., 2013; Zheng et al., 2016) or only diel temperature fluctuations (Gerecht et al., 2011; Zheng & Cardenas, 2018; Zheng et al., 2016). In the present study, we aim to explore complex interactions between river discharge and temperature for river systems with varying degrees of flow alteration across multiple transport time scales.

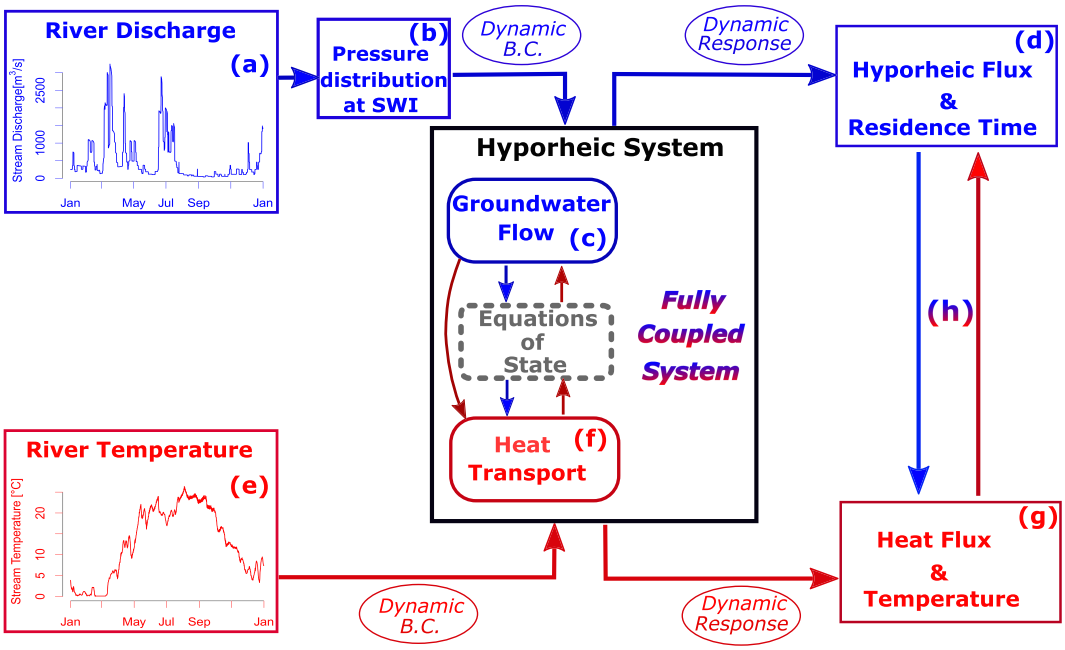

Figure 1. Coupled flow and heat transport in dynamic hyporheic system. River discharge and temperature drive dynamic hyporheic exchange of flow (a–d), represented with the blue color, and energy (e–g), represented with the red color. These exchange processes are coupled in this study (h), represented with the transitional color. B.C. refers to boundary condition.

In the following work, we explore how flow alteration-induced hydrologic changes propagate within hyporheic zones and their implications for heat transport within sediments. We furthermore analyze subsequent impacts on thermal dampening and biogeochemical processes. With this in mind, typical hydrological regimes corresponding to different levels of flow alteration are identified and used as drivers for a hyporheic zone flow and heat transport model, considering temporal variations of river discharge and temperature. The effects of the system properties represented by transport time scales are investigated in the hyporheic exchange processes. Compared to previous studies (Cardenas & Wilson, 2007a; Marzadri et al., 2013; Zheng & Cardenas, 2018; Zheng et al., 2016), this work provides first insights into coupled transient groundwater flow and heat transport processes in hyporheic zones by using natural hydrologic driving forces, providing better understandings to the impact of flow alterations on the hyporheic exchange processes.

2. Methods

2.1. Characterization of Hydrologic Regimes

To find analogies for typical time series of river discharge and temperature under varying degrees of flow alteration, we explore 96 gauging stations in the headwaters of the Mississippi River Basin (MRB). This includes the Missouri (HUC 10), Upper Mississippi (HUC 07), and Ohio (HUC 05) basins. Discharge and temperature time series with 15-min measuring intervals are obtained from the U.S. Geological Survey (USGS) for the period November 2013 to November 2018 (5 years). Site-specific hydrologic, geomorphic, geologic, and anthropogenic information is obtained from the GAGES-II data set (Falcone, 2011).

2.2. Classification of Time Series

Generalizing the effects of flow alteration remains elusive due to the complex feedback mechanisms, varying mode of regulations, regional weather and climate conditions, and local geomorphological settings. To this end, we use K-means cluster analysis, an unsupervised learning technique to find commonalities among gauging stations within the study sites selected (James et al., 2013). K-means partitions a data set of n observations $[\mathbf{x_1}, \mathbf{x_2}, \ldots, \mathbf{x_n}]$ into K distinct and non-overlapping clusters ($C = [C_1, C_2, \ldots C_K]$). An observation $\mathbf{x_i}$ contains information from one or more variables. This method assigns observations to each cluster with the objective of maintaining the objects within a cluster as similar as possible while keeping each cluster as

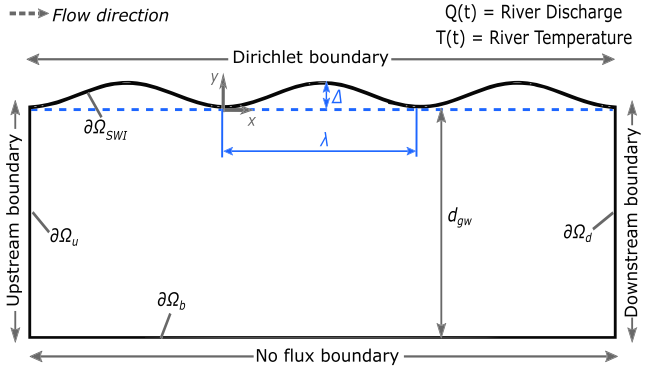

Figure 2. Schematic representation of the sediment domain. The top boundary is sinusoidal with amplitude Δ and wavelength λ. Lateral boundaries are periodic, representing an infinite domain in the longitudinal direction. Bottom boundary is a no flux boundary.

different as possible. For K clusters, this is done with the minimization:

$$\underset{C_1,\ldots,C_k}{\text{minimize}}\left(\sum_{k=1}^{K} W(C_K)\right), \tag{1}$$

where $W(C_K)$ is the within-cluster variation describing the amount by which the observation within a cluster differs from each other. In our analysis, $W(C_K)$ is defined as the squared Euclidean distance among observations.

In our analysis, each observation corresponds to a gauging station, and the variables for the observation are the statistical characteristics of the river discharge and temperature time series (coefficient of variation, autocorrelation, skewness, and kurtosis) and the site-specific characteristics (stream order, drainage area, and dam storage per unit area). In other words, this is a clustering analysis of 11 dimensions. To determine the number of clusters, the silhouette value $s(i)$ proposed by Rousseeuw (1987) is calculated with the R package "factoextra" (Kassambara & Mundt, 2017). In general, partitioning that has the maximum overall average silhouette width, which is the average of the $s(i)$ for all objects i in the whole data set, suggests that the clustering algorithm has discovered a strong clustering structure. This partitioning is selected for understanding the variation and grouping structure of the set of unlabeled data. The grouping results are plotted against each variable to visually identify the most dominant variable that contributes to clustering results.

2.3. Modeling Approach

Typical time series identified with the cluster analysis are used as input for a numerical model to study the coupled groundwater flow and heat transport in hyporheic zones under different degrees of flow alteration.

2.3.1. Model Geometry

To explore the key drivers and controls of the coupled bedform-induced hyporheic flow and heat transport, we use a simple two-dimensional conceptualization (Figure 2). The upper boundary is a sinusoidal sediment-water interface (SWI; $\partial\Omega_{SWI}$) which is assumed periodic with wavelength λ and amplitude Δ. The bottom boundary ($\partial\Omega_b$), located at the depth d_{gw}, is a no flux boundary condition (B.C.), and the lateral boundaries ($\partial\Omega_u$ and $\partial\Omega_d$) are vertical with periodic flow and heat transport conditions, representing an infinite domain in the longitudinal direction (Gomez-Velez et al., 2014; Singh et al., 2019). For simplicity, the bedforms are assumed stationary, and the porous media is homogeneous. COMSOL Multiphysics is used to simulate the water flow and heat transport with a finite element method.

2.3.2. Model for Fully Coupled Water Flow and Heat Transport

Water flow is described by the groundwater flow equation and Darcy's law in a non-deformable porous media (Bear, 1972)

$$\theta\frac{\partial\rho}{\partial t} = \nabla\cdot\left[\rho\frac{\boldsymbol{\kappa}}{\mu}(\nabla p + \rho g\nabla h)\right], \tag{2a}$$

$$h_{SWI}(x, t=0) = h_{IC}(x), \tag{2b}$$

$$p(x, y = Z_{bed}(x), t) = \rho g \quad h_{SWI}(x,t) \quad \text{for } \partial\Omega_{SWI}, \tag{2c}$$

$$p(x=-\lambda, y, t) = p(x=2\lambda, y, t) + \rho g[h_{SWI}(x=-\lambda, t) + h_{SWI}(x=2\lambda, t)] \text{ for } \partial\Omega_u \text{ and } \partial\ \Omega_d, \tag{2d}$$

$$\boldsymbol{\kappa}\frac{\rho g}{\mu}\nabla h = 0 \quad \text{for } \partial\Omega_b, \tag{2e}$$

where t is time [T], θ is porosity [−], $p(\mathbf{x}, t)$ is pressure [$ML^{-1}T^{-2}$], g is gravitational acceleration [LT^{-2}], $\boldsymbol{\kappa}$ is permeability [L^2], ρ is fluid density [ML^{-3}], μ is fluid dynamic viscosity [$ML^{-1}T^{-1}$], h_{IC} is the hydraulic head at $t = 0$ [L], and this initial condition is calculated under steady state, Darcy velocity is $\mathbf{q} = -\frac{\boldsymbol{\kappa}}{\mu}(\nabla p + \rho g\nabla h)$ [LT^{-1}], $Z_{bed}(x) = (\Delta/2)\sin(2\pi x/\lambda)$ is the elevation of the water-sediment interface [L], and $\mathbf{n}$ is an outward

vector normal to the boundary [−]. The aspect ratio (the ratio between amplitude and wavelength Δ/λ) of 0.1 is chosen to represent a ripple bedform (Bridge, 2009). A comprehensive discussion on the effect of local morphology (i.e., aspect ratios) and channel slope on the transient hydraulic pressure propagation within hyporheic zones can be found in Wu et al. (2018).

We prescribe the head distribution at the sediment-water interface (Dirichlet boundary condition) (Wörman et al., 2006):

$$h_{SWI}(x,t) = H_s(t) - Z_{bed}(x) + \frac{2\,h_d(t)}{\Delta}\,Z_{bed}\left(x+\frac{\lambda}{4}\right), \tag{3}$$

where $H_s(t)$ [L] is the time-varying stream stage and $h_d(t)$ is the dynamic head fluctuations (Elliott & Brooks, 1997; Fehlman, 1985)

$$h_d(t) = 0.28\frac{U_s(t)^2}{2g}\begin{cases}\left(\frac{\Delta}{0.34\ H_s(t)}\right)^{3/8} & \text{for}\frac{\Delta}{H_s(t)} \leqslant 0.34\\ \left(\frac{\Delta}{0.34\ H_s(t)}\right)^{3/2} & \text{for}\frac{\Delta}{H_s(t)} > 0.34\end{cases} \tag{4}$$

with the mean velocity $U_s(t) = M^{-1}H_s(t)^{2/3}S^{1/2}$ estimated with the Chezy equation for a rectangular channel with slope S [−] and Manning coefficient M [$L^{-1/3}T$] (Dingman, 2009). In this case, $S = 0.01$ and $M = 0.05$ are used. This conceptualization allows us to capture the hydrodynamic effects of flow passing a bedform with a simple approach based on empirical solutions. Even though the actual process is more complex, a full description would require demanding computational fluid dynamics (CFD) simulations that would limit our ability to explore long time series in multiple systems (Stonedahl et al., 2010). We use this parsimonious simplification, which has been previously used (Wu et al., 2018), to explore the hyporheic response to dynamically changing discharge events.

Heat transport in porous media is described by the heat transport equation (Bejan, 1993; Nield & Bejan, 2013)

$$\frac{\partial T}{\partial t} = \nabla\cdot(\mathbf{D_T}\ \nabla T) - \nabla\cdot(\mathbf{v_T}\ T), \tag{5a}$$

$$T(x,t) = T_s \text{ for } \partial\Omega_{in,SWI}, \tag{5b}$$

$$\mathbf{n}\cdot(\mathbf{D_T}\nabla T) = 0 \text{ for } \partial\Omega_{out,SWI}, \tag{5c}$$

$$T(x=-L,y) = T(x=2L,y) \text{ for } \partial\Omega_u \text{ and } \partial\Omega_d, \tag{5d}$$

$$\mathbf{n}\cdot(\mathbf{v_T}T - \mathbf{D_T}\nabla T) = 0 \text{ for } \partial\Omega_b, \tag{5e}$$

where T is temperature [Θ], $\mathbf{v_T} = (\rho_f\ c_f)/(\rho\ c)\mathbf{q}$ is the thermal front velocity [LT^{-1}], $\mathbf{n}$ is an outward vector normal to the boundary [−], $\mathbf{D_T}$ is the hydrodynamic thermal dispersion tensor [L^2T^{-1}], and $\rho\ c = \theta\ \rho_f\ c_f + (1-\theta)\ \rho_s\ c_s$ is the specific volumetric heat capacity of the fluid-grains media [$ML^{-1}T^{-2}\Theta^{-1}$]. $\rho_f\ c_f$ is the specific volumetric heat capacity of the fluid [$ML^{-1}T^{-2}\Theta^{-1}$], and $\rho_s\ c_s$ is the specific volumetric heat capacity of the solids [$ML^{-1}T^{-2}\Theta^{-1}$]. T_s is the temperature of the water column [Θ], which is the measured river temperature time series. A Dirichlet boundary is used for area along the sediment-water interface where water enters the hyporheic zone, and for water flowing out of the hyporheic zone, a Neumann boundary is used to represent pure convection of heat as described in equations (5b) and (5c). The longitudinal (subscript l) and transversal (subscript t) components of the hydrodynamic thermal dispersion tensor are given by (Bear, 1972; De Marsily, 1986)

$$D_{l,t} = \frac{\kappa_T}{\rho\ c} + \beta_{l,t}|\mathbf{v_T}|, \tag{6}$$

where β_l and β_t are the longitudinal and transverse thermal dispersivity coefficients [L], respectively, and κ_T is the bulk thermal conductivity [$MLT^{-3}\Theta^{-1}$] (Rau et al., 2014; Woodside & Messmer, 1961)

$$\kappa_T = \kappa_f^{\theta}\cdot\kappa_s^{1-\theta}, \tag{7}$$

where κ_f and κ_s are the thermal conductivity of the fluid and solids, respectively.

We couple flow and heat transport with the equations of state (EOS) for dynamic viscosity and density (Furbish, 1996)

$$\mu(T) = m_5\ T^5 + m_4\ T^4 + m_3\ T^3 + m_2\ T^2 + m_1\ T + m_0, \tag{8a}$$

$$\rho(T) = \rho_0 - \rho_0\ \alpha(T - T_0), \tag{8b}$$

where viscosity is in Pa·s, temperature is in ° C, and $m_5 = -3.916 \times 10^{-13}$, $m_4 = 1.300 \times 10^{-10}$, $m_3 = -1.756 \times 10^{-8}$, $m_2 = 1.286 \times 10^{-6}$, $m_1 = -5.895 \times 10^{-5}$, and $m_0 = 1.786 \times 10^{-3}$. The reference density and temperature are $\rho_0 = 1,000\ \mathrm{kg/m^3}$ and $T_0 = 20$ ° C, respectively, and the thermal expansion coefficient is $\alpha = 2.067 \times 10^{-4}$ ° C^{-1}.

2.3.3. Model for Mean Residence Time

For simplicity, we focus on the first moment of the residence time distribution, which is described by Ginn (1999), Gomez and Wilson (2013), and Gomez-Velez et al. (2014)

$$a_1(\mathbf{x}, t) = \int_0^\infty \xi P(\mathbf{x}, t, \xi)\quad \mathrm{d}\xi, \tag{9a}$$

$$\theta \frac{\partial a_1}{\partial t} = \nabla \cdot (\mathbf{D}\nabla a_1) - \nabla \cdot (\mathbf{q} a_1) + \theta a_0, \tag{9b}$$

$$a_1(\mathbf{x}, t) = 0 \quad \text{for } \partial\Omega_{in,SWI}, \tag{9c}$$

$$\mathbf{n} \cdot (\mathbf{D}\nabla a_1) = 0 \quad \text{for } \partial\Omega_{out,SWI}, \tag{9d}$$

$$a_1(x_u, y, t) = a_1(x_d, y, t) \quad \text{for } \partial\Omega_u \text{ and } \partial\Omega_d, \tag{9e}$$

$$\mathbf{n} \cdot (\mathbf{q} a_1 - \mathbf{D}\nabla a_1) = 0 \quad \text{for } \partial\Omega_b, \tag{9f}$$

$$a_1(\mathbf{x}, t = t_0) = a_{1,0}(\mathbf{x}), \tag{9g}$$

where $a_1(\mathbf{x}, t)$ is the first moment [T] of the residence time distribution, ξ is the residence time [T], $P(\mathbf{x}, t, \xi)$ is the residence time distribution [T^{-1}], t is time [T], $\mathbf{x} = (x, y)$ is the spatial location vector, $\mathbf{q}$ is the Darcy flux [LT^{-1}], $a_0 = 1$, and $\mathbf{D} = \{D_{ij}\}$ is the dispersion-diffusion tensor defined as (Bear, 1972)

$$D_{ij} = \alpha_T |\mathbf{q}| \delta_{ij} + (\alpha_L - \alpha_T) \frac{q_i\ q_j}{|\mathbf{q}|} + \frac{\theta}{\xi_m} D_m, \tag{10}$$

where α_T and α_L are the transverse and longitudinal dispersivities, D_m is the effective molecular self-diffusion coefficient, $\xi_m = \theta^{-1/3}$ is the fluid tortuosity estimated by the Millington and Quirk (1961) model, and δ_{ij} is the Kronecker delta function.

2.3.4. Reaction Significance Factor

To quantify the potential of the hyporheic zone to drive biogeochemical reactions, the reaction significance factor (RSF) is calculated. The RSF is the ratio between hyporheic mean residence time and a biogeochemical time scale for the reaction of interest and then weighted by the proportion of discharge passing through the hyporheic zone (Harvey et al., 2013). In our case, the RSF is calculated as the value per unit area of the riverbed by diving the riverbed area of the reach $w \cdot L_c$ in both sides of the equation (denoted by the subscript "a")

$$\mathrm{RSF}_a = \frac{q_{HZ}}{Q} \cdot \frac{\tau_{HZ}}{\tau_{bts}}, \tag{11}$$

where w is river width [L], L_c is characteristic river reach length [L], q_{HZ} is the hyporheic flux out of the hyporheic zone [LT^{-1}], Q is the river discharge [$\mathrm{L^3T^{-1}}$], τ_{HZ} is the hyporheic zone mean residence time [T], and τ_{bts} is a biogeochemical time scale for the reaction of interest [T]. Particularly, we take the denitrification process into consideration; 25th, 50th, and 75th quantiles of typical time scales of denitrification in hyporheic zones (Gomez-Velez & Harvey, 2014; Gomez-Velez et al., 2015) are used in the calculations. A lower value of RSF_a indicates lower denitrification potential.

Table 1
Heat Transport Time Scales [day]

	Reference site	Flow-altered site
t_{c1}	0.05	0.002
t_{c2}	4	0.2
t_{c3}	26	11
t_{c4}	29	28

2.4. Simulation Scenarios

To improve the transferability of the results and compare different systems efficiently, the heat transport time scale is calculated as a function of the size of the bedform (given by the wavelength λ) and the convective and advective heat fluxes (details in Appendix A)

$$t_{hc} = \frac{\lambda^2}{(\mathbf{D_T} + \mathbf{v_c}\lambda)}, \tag{12}$$

where $\mathbf{v_c} = \frac{\rho_f \, c_f}{\rho \, c} \cdot q_c$ and $q_c = K_c \frac{SH_s\Delta^{1/3}}{2gM^2\lambda}$ (Wu et al., 2018). The transport time scale is a simple metric that can be calculated at any location, serving as a useful indicator of the importance of temperature variability.

Simulation scenarios are designed by considering different hyporheic exchange drivers and hyporheic system properties. The hyporheic exchange drivers are characterized by different degrees of flow alterations. Additionally, in the simulation we progressively include temperature time series with increasing degrees of detail, as represented by the frequency components of river temperature (from mean annual, seasonal, to observed time series with 15-min interval). The system properties are described by using different heat transport time scales, which are calculated with equation (12). Four transport time scales are obtained by varying hydraulic conductivity from 10^{-1}, 10^{-3}, 10^{-5}, to 10^{-7} m/s (Table 1). The highest hydraulic conductivity (10^{-1} m/s) is an extreme case. However, we still present it as results in order to gain comprehensive mechanistic understandings. Therefore, in total there are 12 models that are built with considerations of different scenarios of hyporheic exchange drivers and hyporheic system properties discussed above.

2.5. Spectral Analysis and Transfer Function

To evaluate how the hyporheic zone modulates hyporheic exchange drivers, such as river discharge and temperature, we use spectral analysis. Spectral analysis refers to the decomposition of a time domain signal into underlying sine and cosine functions of different frequencies, which allows us to determine those frequencies that appear more important. The spectral analysis is based on Fourier transform. A forward Fourier transform $G(f)$ takes a time domain signal $g(t)$ and transforms it into a frequency domain signal by applying the following integral.

$$G(f) = \int_{-\infty}^{+\infty} g(t) e^{-2\pi i f t} dt, \tag{13}$$

where f is frequency [T^{-1}], t is time [T], and $i = \sqrt{-1}$. The power spectral density, a measure of the proportion of the total variance explained by each frequency (Dobrin & Savit, 1960; Fleming et al., 2002), can be calculated as the square of the modulus of the Fourier transform (Stoica & Moses, 1997)

$$S_G(f) = |G(f)|^2 = G(f) \cdot G^*(f), \tag{14}$$

where $*$ denotes the complex conjugate. Prior to analysis, the linear trend is subtracted to remove any spurious low frequency components, and the power spectrum is smoothed with a Gaussian kernel (R Core Team, 2014).

To quantify how river discharge and temperature signals are retranscribed in the hyporheic zone, a simple relation is used to calculate the experimental transfer function (TF) (Duffy & Gelhar, 1985; Gelhar, 1974; Pedretti et al., 2016; Schuite et al., 2019; Wörman et al., 2012)

$$TF_{temp} = \frac{PSD_{T_{HZ}}}{PSD_{T_s}}, \tag{15}$$

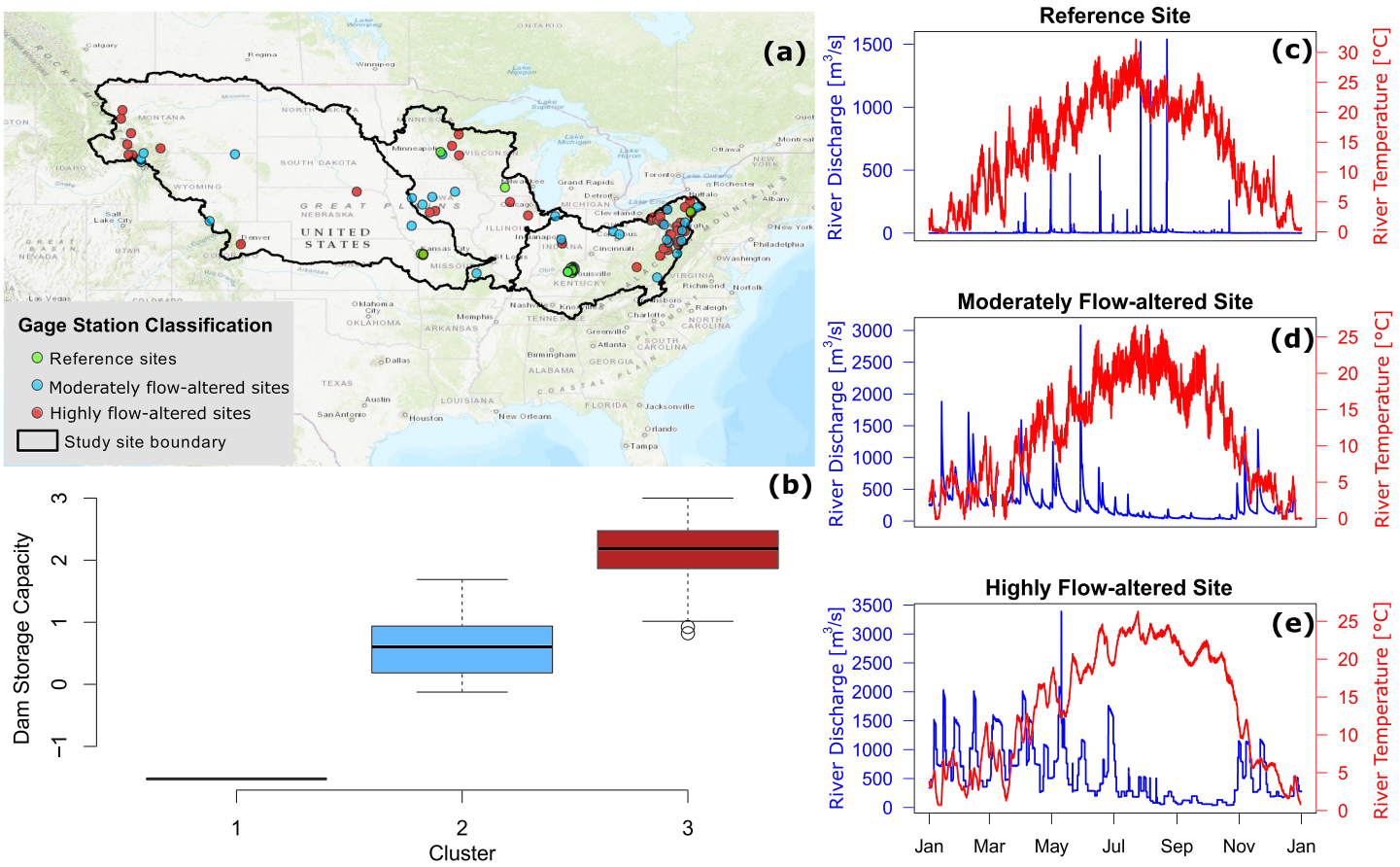

Figure 3. Characterization of hydrologic regimes. (a) Location of 96 USGS gauging stations used for the analysis. (b) Characteristic values of dam storage capacity. Time series of channel discharge (blue) and temperature (red) for typical stations with (c) low, (d) moderate, and (e) high flow alterations.

$$TF_{flow} = \frac{PSD_{HEF}}{PSD_{\mathrm{d}}}, \tag{16}$$

where $PSD_{T_{HZ}}$, PSD_{T_s}, PSD_{HEF}, and PSD_{d} are the power spectral density of temperature of exfiltrating hyporheic exchange fluxes, river temperature, hyporheic exchange fluxes, and river discharge, respectively. In this case, high values of TF correspond to frequencies that are minimally filtered while low values correspond to frequencies that are preferentially filtered.

3. Results and Discussion

3.1. Typical Hydrologic Regimes

The K-means clustering approach identifies three different hydrological regimes across the headwaters region of the Mississippi River Basin (Figure 3). An appropriate number of clusters are determined by using the average silhouette width (supporting information Figure S1). A large average silhouette width suggests a relatively strong clustering structure. Therefore, 3-cluster is chosen as the optimal cluster structure in this analysis. These three subgroups show distinctive ranges of the dam storage capacity (Figure 3b), indicating that this variable plays critical role in the clustering of gauge stations. Figures S2–S4 in the supporting information allow for a visual inspection of the similarities of stations within the same subgroup and differences among subgroups. The main differences among groups are described in the following paragraphs. To reflect the varying levels of flow alteration characterizing the catchment of each gauging station, the three subgroups are named as reference sites, moderately flow-altered sites, and highly flow-altered sites with low, intermediate, and high dam storage per unit area in the catchment, respectively.

Three typical gauging stations are selected to illustrate the nature of each cluster. At the reference site (Figure 3c), river discharge is highly intermittent and characterized by short recession periods; and the

river temperature oscillates at high frequency at daily time scales. As the degree of flow alteration increases (Figure 3d), recession of discharge is more persistent. Discharge of the highly flow-altered site (Figure 3e) shows extended recession periods and fast-onset step-like fluctuations. Furthermore, diel river temperature fluctuations (amplitudes of the time series) are smaller than at the reference site. These patterns are better recognized with more examples presented in Figures S2–S4.

For simplicity and without loss of generality, we focus on the two end-members, reference sites and highly flow-altered sites, to compare the maximum possible differences between sites with and without significant flow alterations. These two groups of sites are hence named as *reference* and *flow-altered* sites thereafter. The comparisons of river discharge, river temperature, hyporheic exchange fluxes, temperature of exfiltrating hyporheic exchange fluxes, hyporheic mean residence time, and heat fluxes between the reference and flow-altered sites are presented in Figure S5. Even though both sites present similar seasonal fluctuation patterns, the daily temporal variations of each metric (Figure S5) at the flow-altered site are much smaller than at the reference site due to flow alterations. The differences between these two sites are further discussed in the following sections.

In conclusion, with the clustering results, two distinct types of hydrological driving forces corresponding to the reference and flow-altered sites are identified. For our analysis, we use the time series of discharge and temperature from USGS gauge stations 06893970 (reference) and 03047000 (flow-altered). These are representative of the reference and flow-altered clusters that are selected because of their long and uninterrupted record during the investigated time window. Notice, however, that stations within a cluster have similar temporal variability (Figures S2–S4). These two sites are used to explore the effect of channel flow and temperature dynamics on hyporheic exchange with numerical simulations in the next step.

3.2. Drivers and Controls of Hyporheic Exchange Dynamics

3.2.1. Hydrological Drivers

To identify the relative importance of discharge and temperature variations on the exchange processes at the sediment-water interface, we perform a series of numerical experiments where we progressively include temperature time series with increasing degrees of detail, as represented by the frequency components of river temperature. In the first scenario, the hyporheic response metrics (including hyporheic exchange fluxes, temperature of exfiltrating hyporheic exchange fluxes, mean residence time, and RSF_a) are simulated with a constant mean annual temperature (black solid lines in Figure 4) which results in constant viscosity (μ) and density (ρ) (equation (8)). In the second scenario, the same hyporheic metrics are simulated with a seasonal temperature time series (green solid lines). In the third scenario, the simulation is with the original river temperature time series, based on observations at 15-min intervals (red solid lines). In the second and third scenarios, viscosity (μ) and density (ρ) vary with temperature over time.

At the reference site, hyporheic exchange fluxes simulated under the assumption of constant mean annual temperature follow the patterns of the river discharge time series (the gray solid line), and the peaks are coinciding with the discharge peaks (Figure 4a). In the second scenario, hyporheic exchange fluxes exhibit prominent annual periodicity with only a few peaks corresponding to extreme discharge events. In the third scenario, where the measured temperature including full frequency range is used as the model input, hyporheic exchange fluxes present both annual and daily fluctuations. However, strong fluctuations in hyporheic exchange fluxes corresponding with high discharge events are not prominent. These progressively decreasing hyporheic exchange flux fluctuations that are coinciding with high discharge events, when gradually including more details in temperature driver (as presented in Scenarios 1 to 3), indicate that temperature has a direct control in determining hyporheic flow dynamics. The temperature of the exfiltrating hyporheic exchange fluxes simulated using the original observed time series is dampened compared to the river temperature (Figure 4c). Mean residence time simulated with the constant mean annual and seasonal temperatures only shows residence time peaks coinciding with discharge peaks without capturing the diel fluctuations. Mean residence time simulated with observed original temperature time series shows clear diel fluctuations with fewer residence time peaks coinciding with discharge peaks (Figure 4e). This results from the direct control that temperature plays in dynamic hyporheic exchange process. The RSF_a, calculated with 50th quantile of typical time scales of denitrification, present relatively large variation range across 5 orders of magnitude; however, there is no apparent difference among the RSF_a calculated with the three temperature scenarios (Figure 4g).

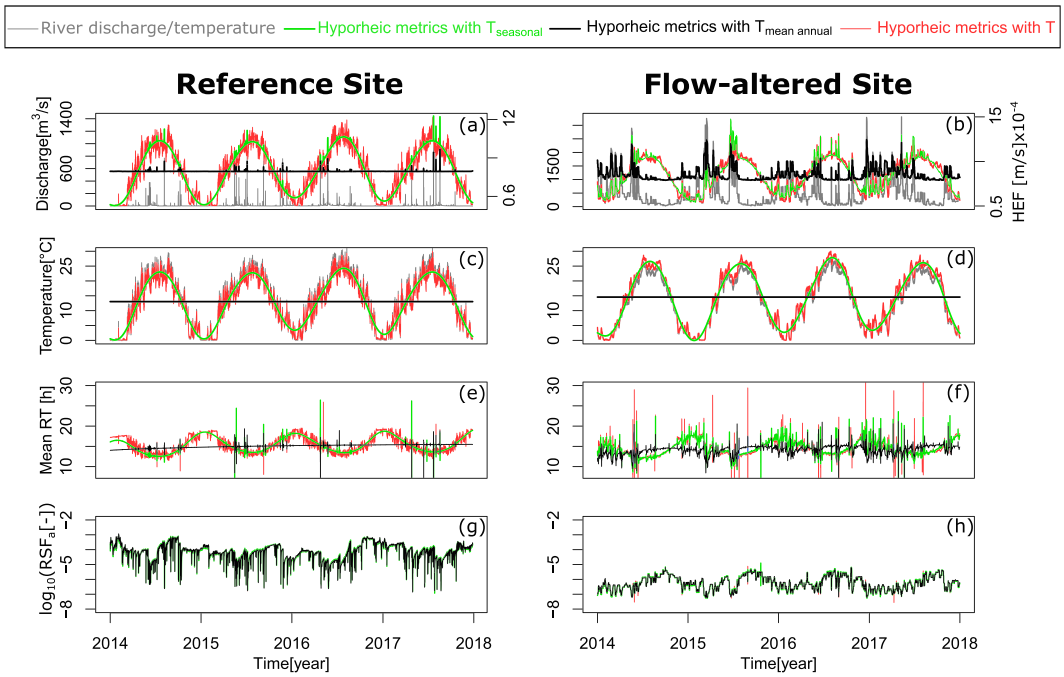

Figure 4. Effect of river temperature on hyporheic responses metrics. Hyporheic exchange fluxes (HEF), temperature of exfiltrating hyporheic exchange fluxes, mean residence time (RT), and reaction significance factor (RSF_a) simulated with constant mean annual temperature ($T_{\text{mean annual}}$), seasonal temperature dynamics (T_{seasonal}), and original river temperature time series (T), respectively, at the reference site (a, c, e, g) and at the flow-altered site (b, d, f, h). Heat transport scale t_{c2} is used in the calculation of presented results.

Nevertheless, at the flow-altered site, the fluctuations of hyporheic exchange fluxes induced by high discharge events are evident in all three temperature scenarios (Figure 4b). Compared with the reference site, both river temperature and the temperature of exfiltrating hyporheic exchange fluxes present less fluctuations in daily scales (Figure 4d). Mean residence time shows more fluctuations that are corresponding with discharge events (Figure 4f). RSF_a shows step-like fluctuations and varies across 2 orders of magnitude (Figure 4h), which is much smaller than at the reference site, indicating less significant denitrification potentials.

Compared with using only mean annual temperature (black solid lines in Figure 4), including more characteristic frequencies of temperature time series (i.e., the annual or both annual and daily frequencies) in the simulation contributes to more extensive hyporheic dynamic responses at both the reference and flow-altered sites (green and red solid lines in Figure 4). This results from the temperature-dependent transport processes as described in EOS (equation (8)). The viscosity μ is decreasing with increasing temperature, which leads to an increase of hydraulic conductivity, $K = \kappa g\rho/\mu$, hence an increase of hyporheic exchange fluxes. Temperature dependence of density is small and is in most cases negligible (Fetter, 2001). These dynamics contribute to a strong temperature dependency of the hyporheic response to changing river discharge and temperature.

At the flow-altered site, the estimated hyporheic exchange fluxes capture the dynamic oscillations reasonably well by using only seasonal temperature fluctuations (green solid lines in Figures 4a and 4b). This is because storm-scale and diel temperature fluctuations in the flow-altered systems are subdued and the dynamic discharge is more dominant in determining the hyporheic responses (Figure 3e). Therefore, in this case omitting storm-scale and diel fluctuations has less impact on estimating hyporheic exchange fluxes. On the contrary, at the reference site, the discharge is more intermittent, with pronounced diel temperature oscillations; hence, the hyporheic exchange is more affected by temperature fluctuations than at the flow-altered site. Therefore, when estimating hyporheic exchange fluxes and temperature of the exfiltrating hyporheic exchange fluxes, the diel fluctuations can be omitted in systems where daily temperature fluctuations are modified with reduced amplitude both naturally and anthropogenically. Under these conditions,

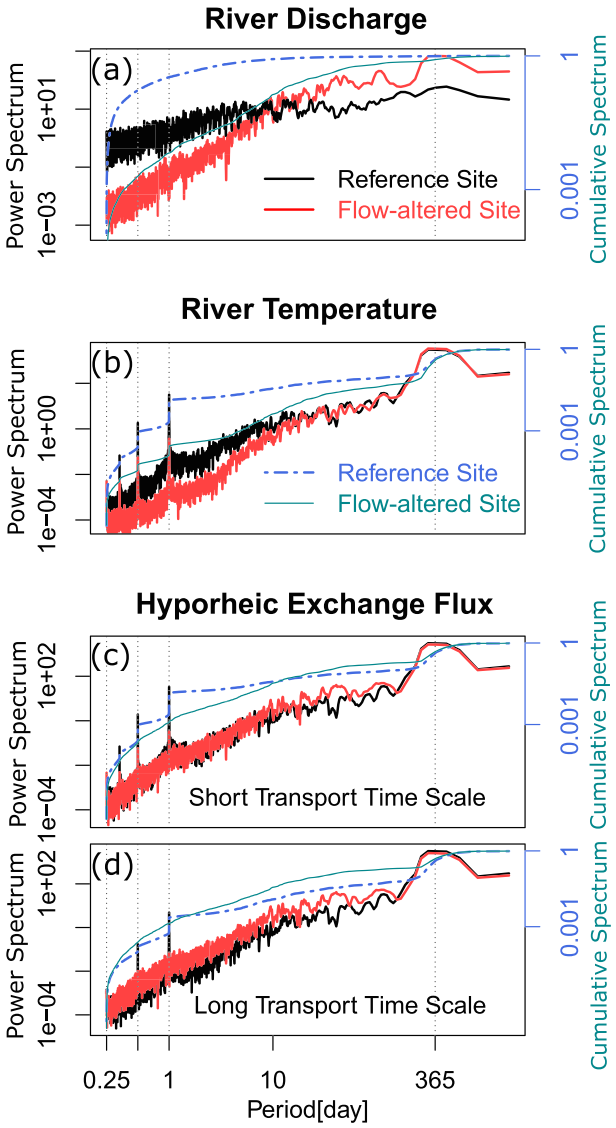

Figure 5. Spectral analysis of hyporheic exchange processes. Power spectrum and cumulative power spectrum of (a) river discharge, (b) river temperature, and hyporheic exchange fluxes simulated with (c) short transport time scale (t_{c1}) and (d) long transport time scale (t_{c3}) at the reference and flow-altered sites. The cutout of period at 0.25 [day] is determined by the Nyquist frequency of the simulated outputs.

hyporheic exchange fluxes and their temperature simulated only with seasonal temperature variations (i.e., the green solid lines in Figures 4b and 4d) can thus serve as adequate approximations.

To better understand what drives the dynamic responses of hyporheic exchange fluxes, we explore the hyporheic exchange input and output signals in the frequency domain. The power spectrum for discharge, temperature, and hyporheic exchange fluxes simulated with two different heat transport time scales is shown in Figures 5a–5d for both the reference and flow-altered sites. Cumulative power spectrum is plotted in each case to highlight the total frequency drop at characteristic frequency range. The discharge time series do not have characteristic frequencies in daily time scales (i.e., peaks in the power spectrum), and the cumulative frequencies are smoothly decreasing, indicating no dominant frequency (Figure 5a). It is noteworthy that this discharge pattern is not generalized for all the flow-altered system. For instance, a weekly frequency was observed in regulated system by Zmijewski and Wörman (2016), which indicates that the frequency responses of the discharge depend on the regulation strategy. This variability is further discussed in section 3.3. On the other hand, temperature, at both the reference and flow-altered sites, shows clear power

spectrum peaks in annual and daily frequencies (Figure 5b). At the reference site, the cumulative temperature power spectrum has an evident step drop at each annual and daily frequencies, whereas the cumulative power spectrum of the flow-altered site is smoother across the whole frequency range, indicating subdued fluctuation patterns.

The power spectrum of the hyporheic exchange fluxes simulated with the shortest transport time scale of t_{c1} for both sites presents similar slopes and frequency signatures in annual and daily frequencies (Figure 5c). However, in the daily frequency range, the power spectrum of hyporheic exchange fluxes at the reference site simulated with longer transport time scale of t_{c3} shows almost no characteristic peaks (indicated by the missing peaks at the daily periods of the red solid line in Figure 5d).

Previous studies have shown that hyporheic exchange fluxes can be substantially modified by viscosity and density changes due to temperature variation (Cardenas & Wilson, 2007a). However, to the best of the authors knowledge, this is the first time that a detailed analysis of coupled groundwater flow and heat transfer problem has been performed considering natural hydrologic driving forces under transient conditions. Figure 4 shows the importance of incorporating temperature-dependent process into hyporheic exchange estimations. Simulated hyporheic exchange fluxes estimated from a constant mean annual temperature lose the variability inherited from the natural river temperature fluctuations. The annual and daily fluctuations occurring in the real world are completely absent without taking temperature dependency of the hyporheic exchange process into consideration, which may introduce large uncertainties in hyporheic exchange rate and mean residence time estimations.

Additionally, the large temperature variations in natural fluvial environment also imply the importance of including temperature dependency in hyporheic zone studies. Cardenas and Wilson (2007a) found viscosity has larger sensitivity in low temperature range (i.e., 6 ± 5 °C) compared with higher temperature range (i.e., 20 ± 5 °C). In the present study, the temperature varies from 0 to 32 °C in the reference site and 0 to 28 °C in the flow-altered site, covering both low and high temperature ranges. With this temperature variation (approximately from 0 to 30 °C), viscosity decreases by 45% and hydraulic conductivity increases by 220%. Impacts on hyporheic exchange due to these changes should not be neglected.

Results shown in frequency domain further strengthen the importance of temperature signal inheritance by the hyporheic system. The power spectrum of hyporheic exchange fluxes, as an important system response, shows prominent peaks in daily frequency range (Figures 5c and 5d). Importantly, these peaks are only observed in the temperature power spectrum (Figure 5b) but not in the river discharge power spectrum (Figure 5a). This indicates that the temporal variability of hyporheic exchange fluxes is strongly affected by the variability in river temperature, and therefore, analysis that ignores thermal effects will lead to significant inaccuracies.

The slope of the PSD reflects the manner of organization of the time series (Zmijewski & Wörman, 2016). A horizontal power spectrum represents a white noise process (Zhang & Schilling, 2004). The flow-altered sites present a steeper discharge power spectrum slope (Figure 5a), which is consistent with the time series that has a more organized pattern (the step-like fluctuations in the discharge time series in Figure S5b). On the other hand, the fluctuations in river discharge at the reference site are closer to white noise. Although in the time domain there are more discernible fluctuations of river temperature at the reference site than at the flow-altered site (Figures S5a and S5b), in the frequency domain both sites present the same frequency signatures and similar power spectrum slopes with only small deviations in the high-frequency range (Figure 5b). This observation is in line with Ferencz and Cardenas (2017) who found that the seasonal diel temperature range is relatively insensitive to changes in discharge. Despite these differences in driving forces, river discharge and temperature, power spectrum slopes of hyporheic exchange fluxes show similar patterns between the reference and flow-altered sites, which indicates a similar scaling property in the system response. A noticeable difference between the two hyporheic systems with different transport time scale (t_{c1} and t_{c3}) is that the daily frequency signatures disappeared in the flow-altered system with longer transport time scale (red line in Figure 5d). This indicates that with longer transport time scale, the hyporheic system presents a stronger dampening effect. The daily peaks remain in the power spectrum of the hyporheic flux at the reference site due to the stronger diel temperature oscillations at the reference site.

Similar to the fractal filter property observed between groundwater recharge input and aquifer hydraulic head response (Zhang & Schilling, 2004), the hyporheic system also behaves as a fractal filter producing temporal scaling of hyporheic exchange fluxes regardless of a white noise or a fractal discharge input.

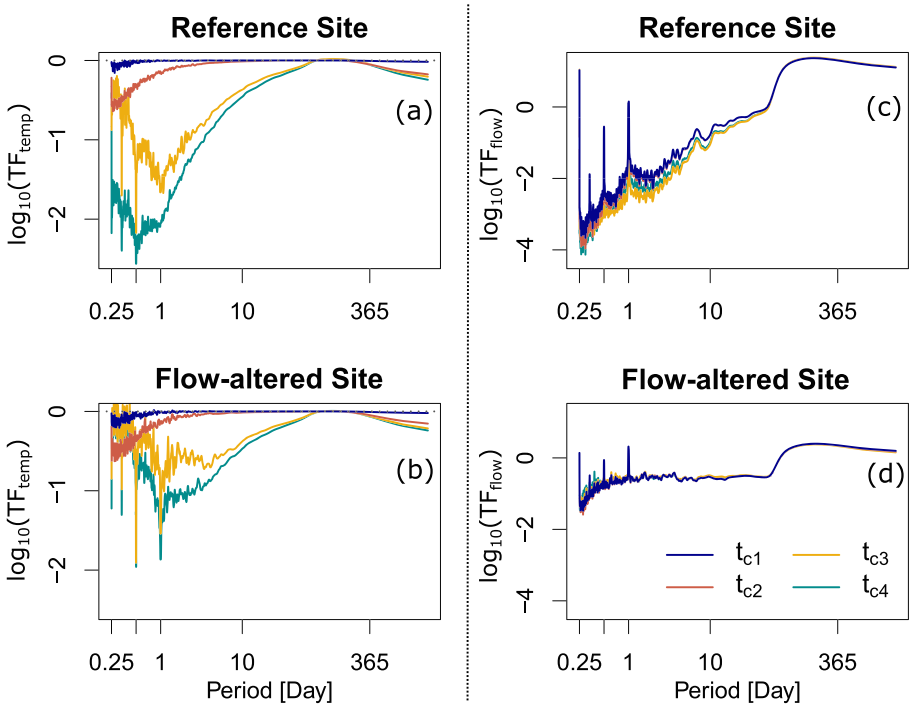

Figure 6. Experimental transfer functions in different hyporheic systems. Temperature transfer functions (TF_{temp}) under four transport time scales (a) at the reference site and (b) at the flow-altered site. Flow transfer functions (TF_{flow}) under four transport time scales (c) at the reference site and (d) at the flow-altered site.

3.2.2. Sediment Property Impacts on Hyporheic Exchange

Experimental transfer functions are introduced to further understand the hyporheic dampening ability of the input fluctuations. To account for the variety of the sediment properties, four different transport time scales (Table 1) are considered in the experimental transfer functions between river temperature and temperature of exfiltrating hyporheic exchange fluxes and between discharge and hyporheic exchange fluxes for each site. The shape of the experimental transfer function directly relates to the system efficiency to dampen input signals. A flat transfer function indicates a constant dampening efficiency of the input signals across the whole frequency range exploredm, whereas a transfer function with steep slope indicates a large increase or decrease in dampening capacity of hyporheic zones with increasing frequency.

The temperature transfer functions which are calculated as ratio between temperature of exfiltrating hyporheic exchange fluxes and river temperature (equation (15)) present distinctive patterns in each scenario simulated with different transport time scales (Figures 6a and 6b). With the shortest transport time scale (t_{c1}), the temperature transfer functions of both sites are close to a horizontal line with the value of 1, suggesting that across the explored frequency range, the temperature signals of the exfiltrating hyporheic exchange fluxes remain almost unchanged in both frequency composition and spectral power. With longer transport time scales, nonlinear trends are observed. With transport time scales t_{c3} and t_{c4}, the drop at the midfrequency domain indicates an increase of the dampening efficiency; the rise at the high-frequency domain indicates a decrease of efficiency. On the other hand, the dampening efficiency in the system with t_{c2} (the red solid lines for both the reference and flow-altered sites in Figure 6) only shows an increase of dampening efficiency around daily frequency, and the trend continues toward the high-frequency domain.

These variations of the temperature transfer functions (TF_{temp}) evidence that, in the Fourier domain and under the same input river temperature, the temperature signal of exfiltrating hyporheic exchange fluxes is closely dependent on the heat transport time scales. The longer the transport time scale, the stronger the hyporheic zone dampens the input signals. Hyporheic dampening efficiency is not constant throughout the explored frequency domain. In general, noticeable signal dampening occurs when approaching to the high-frequency domain. However, this tendency is obviously not linear. The nonlinearity suggests that the hyporheic system does not hold the same efficiency (which the transfer function would have been

a horizontal line) and the same efficiency changing rate (which the transfer function would have been slope invariant) in dampening input temperature signals. The highest dampening efficiency is around the daily frequency.

Differing from the temperature transfer functions, the flow transfer functions, which is calculated as a ratio between hyporheic exchange fluxes and river discharge (equation (16)), do not show much differences across the four transport time scales explored (Figures 6c and 6d). However, comparing between the flow-altered and reference sites, the flow transfer functions of the flow-altered site are relatively flat, whereas the flow transfer functions of the reference site show steeper slopes. This observation suggests that for the reference site the hyporheic dampening efficiency of the input signal is increasing with higher signal frequencies; on the other hand, the efficiency of the flow-altered site remains almost constant. Similar as the flow transfer function, the variability of the temperature transfer function is larger at the reference site than at the flow-altered site, which also indicates a reduced dampening efficiency due to flow alteration at the flow-altered site.

It's worth noticing that the temperature transfer function exhibits downward peaks with t_{c3} and t_{c4} but upward peaks in flow transfer function at daily frequencies. This is because diel fluctuations are reduced in the temperature of the exfiltrating hyporheic exchange fluxes as the output of the hyporheic zones compared with the river temperature as the input, while the diel fluctuations which are absent in the input discharge signals are attached in the hyporheic exchange fluxes as the output. This difference further confirms the conclusion we made earlier that the hyporheic exchange fluxes inherit the frequency signatures from the river temperature. The absence of downward peaks in temperature transfer function with t_{c1} and t_{c2} is due to the short transport time scales which leave the hyporheic system no time to dampen the input signals. Also, comparing between the reference and flow-altered sites, both the downward and upward peaks are more prominent in the reference sites, highlighting that the potential of hyporheic zones as a flow and temperature buffer is reduced by flow alteration. In conclusion, the dampening effect of the hyporheic zone varies with frequency, and its efficiency is modulated by the transport time scales as well as by flow alterations.

3.2.3. Biogeochemical Implications

For simplicity, the RSF_a is calculated for the scenarios with the shortest (t_{c1}) and longest transport time scales (t_{c4}) for both the reference and flow-altered sites (Figures 7a and 7c). The RSF_a at the reference site is higher than the RSF_a at the flow-altered site by about 2 orders of magnitude. This is also indicated by the density plots which show two distinct mean values in each transport time scenario (Figures 7b and 7d). However, the differences between the two transport time scales are negligible (Figure S6). This is because q_{HZ} in the numerator of RSF_a is proportional to the hydraulic conductivity, whereas τ_{HZ} is proportional to the reciprocal of hydraulic conductivity (equations (A15) and (A16) in Wu et al., 2018). Therefore, the effect of different hydraulic conductivity cancels out. And in our case, the transport time scale is only controlled by hydraulic conductivity; hence, the RSF_a shows similar patterns between the reference and flow-altered sites. However, if the transport time scale is also modified by other parameters (in equation (12)), the difference between the reference and flow-altered systems cannot be ignored.

At the flow-altered site, the step-shape RSF_a and generally lower denitrification potentials than at the reference site are caused by flow alteration, highlighting the negative effects of flow alterations on the denitrification potential of river systems. The biogeochemical time scale (τ_{bts} in equation (11)) depends on the reaction of interest. Here we focus on denitrification as an example of wide interest. Notice, however, that for a given reaction (a set value of τ_{bts}), the RSF_a of the flow-altered sites remains lower than the one in the reference sites.

3.3. Study Limitations

The main objective of this study is not to simulate hyporheic exchange in perfect details but rather to capture the essence of hyporheic exchange under coupled groundwater flow and heat transport process with transient flow and temperature boundary conditions. Here we briefly discuss the model limitations on assumptions and boundary conditions. A more detailed critical review on main assumptions and limitations on model dimensionality, morphological setting, and groundwater conditions is presented in Wu et al. (2018).

In the present study, only bedform-induced hyporheic exchange is investigated. However, lateral hyporheic exchange with meander bends, floodplain water bodies, and buried paleochannels also play a significant role in exchange of flow, energy, and solute, which by all means should not be neglected (Buffington &

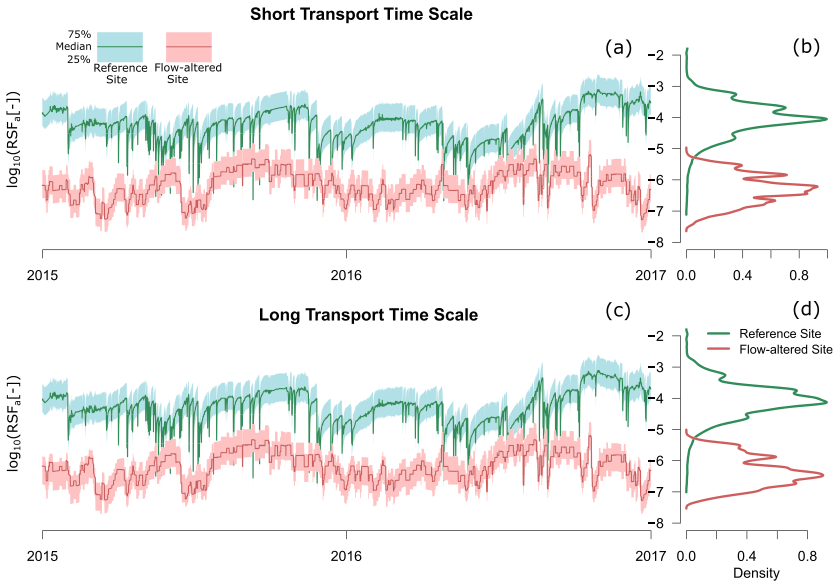

Figure 7. Reaction significance factors per unit area (RSF_a) for denitrification potentials. RSF_a and density plots for the reference (green) and flow-altered (red) sites under (a and b) short transport time scale (t_{c1}) and (c and d) long transport time scale (t_{c4}). A smaller value of the RSF_a means that the reaction potential is lower.

Tonina, 2009; Gomez-Velez et al., 2017). However, the lateral hyporheic exchange processes significantly differ in scales and exchange mechanics from bedform-induced hyporheic exchange. Therefore, future research focusing on the coupled groundwater and heat transport in lateral hyporheic exchange processes is needed to comprehensively understand hyporheic exchange processes.

Accurately representing the momentum transfer induced by turbulent flow between the main channel and the adjacent sediment requires detailed computational fluid dynamic model that solves the full Navier-Stokes equations, but computationally efficient approaches are also necessary for exploring long time series in multiple systems. The calculated velocity in the water column is simplified by ignoring the turbulent flow. This simplification allows us to simulate hyporheic exchange for a long temporal scale; however, the local streambed pressure anomalies associated with turbulent flow, such as hydraulic jumps, will be disregarded (Grant et al., 2018; Trauth et al., 2013). Consequently, heat distribution in hyporheic zones is also likely to be altered.

The boundary conditions used in the simulations are calculated with the observed river discharge and temperature time series. These typical hydrologic regimes are identified with cluster analysis. The observed river discharge and temperature time series share commonalities within each cluster. For instance, river discharge is highly intermittent and characterized by short recession periods at the reference site. As the degree of flow alteration increases, recession of discharge is more persistent and fluctuations are more step-like; diel river temperature fluctuations become smaller than at the reference site. Although K-means method is carried out with the objective of grouping stations within a cluster as similar as possible while keeping each cluster as different as possible, the stations within each subgroup are not identical. Their temporal behavior, however, is very similar (Figures S2–S4).

There is variability due to the time series selection. We use a long 5-year time series that captures a myriad of events representing the complex temporal variability observed in natural system. Given the computational demand of the approach, only two sites are analyzed. However, the differences induced by using another representative observation in the same subgroup as model inputs will not be as significant as the differences among the three subgroups due to the apparently distinct characteristics of the driving forces (discharge and temperature) categorized by the cluster analysis.

4. Conclusions

Transient river discharge and temperature drive dynamic hyporheic exchange of flow and energy. In this study, we systematically explore the coupled hyporheic system responses to the drivers (river discharge

and temperature), which are characterized by different degrees of flow alteration, and modulators described by hydraulic and thermal properties of the sediment. Hyporheic exchange fluxes inherit the daily spectral signatures from river temperature fluctuations, and noticeably, these signatures are absent in discharge, indicating a direct control of temperature on hyporheic exchange processes. Omitting flow temperature variability results in substantial inaccuracies in hyporheic exchange rate and mean residence time estimation.

Hyporheic zones dampen the river temperature fluctuations. This dampening effect increases with higher frequency of temperature fluctuations and is enhanced with longer system's transport time scale. This finding underlines their frequently described functioning as thermal refugia, protecting aquatic communities from extreme thermal disturbances. However, alteration of river flow causes a reduction in the potential of hyporheic zones to buffer both temperature and solutes (i.e., denitrificaition). Our findings highlight the necessity of including temperature-dependent processes into hydrodynamic studies and upscaling models of hyporheic exchange.

Appendix A: Characteristic Time Scale for Heat Transport

$$\frac{\partial T}{\partial t} = \nabla \cdot (\mathbf{D_T}\ \nabla T) - \nabla \cdot (\mathbf{v_T}\ T), \tag{A1}$$

$$\frac{\Delta T}{t_c} = \frac{1}{\lambda}\mathbf{D_T}\frac{\Delta T}{\lambda} + \frac{1}{\lambda}\mathbf{v_c}\ \Delta T, \tag{A2}$$

$$\frac{1}{t_c} = \frac{1}{\lambda^2}\mathbf{D_T} + \frac{\lambda}{\lambda^2}\mathbf{v_c}. \tag{A3}$$

Hence, characteristic time scale for heat transport is given by

$$t_c = \frac{\lambda^2}{(\mathbf{D_T} + \mathbf{v_c}\lambda)}, \tag{A4}$$

where

$$v_c = \frac{\rho_f\ c_f}{\rho\ c}.q_c, \tag{A5}$$

$$\mathbf{D_T} = \frac{\kappa_T}{\rho\ c}, \tag{A6}$$

$$\kappa_T = k_f^{\theta}.k_s^{1-\theta}, \tag{A7}$$

$$\rho\ c = \theta\ \rho_f\ c_f + (1-\theta)\ \rho_s\ c_s, \tag{A8}$$

and characteristic q_c is the same as we calculated previously (Appendix 1 in Wu et al., 2018)

$$q_c = K_c\frac{SH_s\Delta^{1/3}}{2gM^2\lambda}. \tag{A9}$$

Acknowledgments
This study has received funding from the European Union's Horizon 2020 research and innovation program under Marie Sklodowska-Curie Grant Agreements 641939 (HypoTRAIN) and 734317 (HiFreq). Additional funding was granted by the German Research Foundation (DFG) for the Research Training Group under GRK 2032/1 (Urban Water Interfaces). J. D. Gomez-Velez is funded by the U.S. National Science Foundation (Award EAR 1830172) and the U.S. Department of Energy, Office of Biological and Environmental Research (BER), as part of BER's Subsurface Biogeochemistry Research Program (SBR). This contribution originates from the SBR Scientific Focus Area (SFA) at the Pacific Northwest National Laboratory (PNNL). All data required to reproduce the figures in this paper are available on the database of Leibniz-Institute of Freshwater Ecology and Inland Fisheries (https://www.igb-berlin.de/freshwater-research-and-environmental-database).

References

Abril, M., Muñoz, I., Casas-Ruiz, J. P., Gómez-Gener, L., Barceló, M., Oliva, F., & Menéndez, M. (2015). Effects of water flow regulation on ecosystem functioning in a Mediterranean river network assessed by wood decomposition. *Science of the Total Environment*, *517*, 57–65.

Anderson, M. P. (2005). Heat as a ground water tracer. *Groundwater*, *43*(6), 951–968.

Bear, J. (1972). *Dynamics of fluids in porous media*. New York: American Elsevier Publishing.

Bejan, A. (1993). *Heat transfer*. New York: John Wiley & Sons English.

Boano, F., Harvey, J. W., Marion, A., Packman, A. I., Revelli, R., Ridolfi, L., & Wörman, A. (2014). Hyporheic flow and transport processes: Mechanisms, models, and biogeochemical implications. *Reviews of Geophysics*, *52*, 603–679. https://doi.org/10.1002/2012RG000417

Boano, F., Revelli, R., & Ridolfi, L. (2013). Modeling hyporheic exchange with unsteady stream discharge and bedform dynamics. *Water Resources Research*, *49*, 4089–4099. https://doi.org/10.1002/wrcr.20322

Bridge, J. S. (2009). *Rivers and floodplains: Forms, processes, and sedimentary record*. Oxford: John Wiley & Sons.

Buffington, J. M., & Tonina, D. (2009). Hyporheic exchange in mountain rivers II: Effects of channel morphology on mechanics, scales, and rates of exchange. *Geography Compass*, *3*(3), 1038–1062.
Burkholder, B. K., Grant, G. E., Haggerty, R., Khangaonkar, T., & Wampler, P. J. (2008). Influence of hyporheic flow and geomorphology on temperature of a large, gravel-bed river, Clackamas River, Oregon, USA. *Hydrological Processes: An International Journal*, *22*(7), 941–953.
Caissie, D. (2006). The thermal regime of rivers: A review. *Freshwater biology*, *51*(8), 1389–1406.
Cardenas, M. B., & Wilson, J. L. (2007a). Effects of current–bed form induced fluid flow on the thermal regime of sediments. *Water Resources Research*, *43*, W08431. https://doi.org/10.1029/2006WR005343
Cardenas, M. B., & Wilson, J. L. (2007b). Exchange across a sediment–water interface with ambient groundwater discharge. *Journal of Hydrology*, *346*(3-4), 69–80.
Cardenas, M. B., Wilson, J., & Zlotnik, V. A. (2004). Impact of heterogeneity, bed forms, and stream curvature on subchannel hyporheic exchange. *Water Resources Research*, *40*, W08307. https://doi.org/10.1029/2004WR003008
Constantz, J. (1998). Interaction between stream temperature, streamflow, and groundwater exchanges in alpine streams. *Water Resources Research*, *34*(7), 1609–1615.
Constantz, J., Thomas, C. L., & Zellweger, G. (1994). Influence of diurnal variations in stream temperature on streamflow loss and groundwater recharge. *Water Resources Research*, *30*(12), 3253–3264.
De Marsily, G. (1986). *Quantitative hydrogeology: Groundwater hydrology for engineers* (1edition). London: Academic Press.
Dingman, S. L. (2009). *Fluvial hydraulics*. Oxford; New York: Oxford University Press.
Dobrin, M. B., & Savit, C. H. (1960). *Introduction to geophysical prospecting* (Vol. 4). New York: McGraw-hill.
Duffy, C. J., & Gelhar, L. (1985). A frequency domain approach to water quality modeling in groundwater: Theory. *Water Resources Research*, *21*(8), 1175–1184.
Elliott, A. H., & Brooks, N. H. (1997). Transfer of nonsorbing solutes to a streambed with bed forms: Theory. *Water Resources Research*, *33*(1), 123–136.
Falcone, J. A. (2011). GAGES-II: Geospatial attributes of gages for evaluating streamflow: US Geological Survey.
Fehlman, H. M. (1985). Resistance components and velocity distributions of open channel flows over bedforms (Ph.D. Thesis).
Ferencz, S. B., & Cardenas, M. B. (2017). Diel stream temperature regimes of Bukovsky regions of the conterminous United States. *Geophysical Research Letters*, *44*, 2264–2271. https://doi.org/10.1002/2017GL072641
Fetter, C. W. (2001). *Applied hydrogeology*. New Jersey: Waveland Press.
Fleming, S. W., Marsh Lavenue, A., Aly, A. H., & Adams, A. (2002). Practical applications of spectral analysis to hydrologic time series. *Hydrological Processes*, *16*(2), 565–574.
Furbish, D. J. (1996). *Fluid physics in geology: An introduction to fluid motions on Earth's surface and within its crust*. Cary: Oxford University Press.
Gelhar, L. (1974). Stochastic analysis of phreatic aquifers. *Water Resources Research*, *10*(3), 539–545.
Gerecht, K. E., Cardenas, M. B., Guswa, A. J., Sawyer, A. H., Nowinski, J. D., & Swanson, T. E. (2011). Dynamics of hyporheic flow and heat transport across a bed-to-bank continuum in a large regulated river. *Water Resources Research*, *47*, W03524. https://doi.org/10.1029/2010WR009794
Ginn, T. R. (1999). On the distribution of multicomponent mixtures over generalized exposure time in subsurface flow and reactive transport: Foundations, and formulations for groundwater age, chemical heterogeneity, and biodegradation. *Water Resources Research*, *35*(5), 1395–1407.
Gomez, J., & Wilson, J. (2013). Age distributions and dynamically changing hydrologic systems: Exploring topography-driven flow. *Water Resources Research*, *49*, 1503–1522. https://doi.org/10.1002/wrcr.20127
Gomez-Velez, J. D., & Harvey, J. W. (2014). A hydrogeomorphic river network model predicts where and why hyporheic exchange is important in large basins. *Geophysical Research Letters*, *41*, 6403–6412. https://doi.org/10.1002/2014GL061099
Gomez-Velez, J. D., Harvey, J. W., Cardenas, MBayani, & Kiel, B. (2015). Denitrification in the Mississippi River network controlled by flow through river bedforms. *Nature Geoscience*, *8*(12), 941.
Gomez-Velez, J. D., Krause, S., & Wilson, J. L. (2014). Effect of low-permeability layers on spatial patterns of hyporheic exchange and groundwater upwelling. *Water Resources Research*, *50*, 5196–5215. https://doi.org/10.1002/2013WR015054
Gomez-Velez, J. D., Wilson, J., Cardenas, M., & Harvey, J. (2017). Flow and residence times of dynamic river bank storage and sinuosity-driven hyporheic exchange. *Water Resources Research*, *53*, 8572–8595. https://doi.org/10.1002/2017WR021362
Gooseff, M. N. (2010). Defining hyporheic zones—Advancing our conceptual and operational definitions of where stream water and groundwater meet. *Geography Compass*, *4*(8), 945–955.
Grant, S. B., Gomez-Velez, J. D., & Ghisalberti, M. (2018). Modeling the effects of turbulence on hyporheic exchange and local-to-global nutrient processing in streams. *Water Resources Research*, *54*, 5883–5889. https://doi.org/10.1029/2018WR023078
Harvey, J. W., Böhlke, J. K., Voytek, M. A., Scott, D., & Tobias, C. R. (2013). Hyporheic zone denitrification: Controls on effective reaction depth and contribution to whole-stream mass balance. *Water Resources Research*, *49*, 6298–6316. https://doi.org/10.1002/wrcr.20492
Harvey, J. W., Wagner, B. J., & Bencala, K. E. (1996). Evaluating the reliability of the stream tracer approach to characterize stream-subsurface water exchange. *Water Resources Research*, *32*(8), 2441–2451.
Hester, E. T., Doyle, M. W., & Poole, G. C. (2009). The influence of in-stream structures on summer water temperatures via induced hyporheic exchange. *Limnology and Oceanography*, *54*(1), 355–367.
James, G., Witten, D., Hastie, T., & Tibshirani, R. (2013). *An introduction to statistical learning* (Vol. 112). New York: Springer.
Kalbus, E., Schmidt, C., Molson, J., Reinstorf, F., & Schirmer, M. (2009). Influence of aquifer and streambed heterogeneity on the distribution of groundwater discharge. *Hydrology and Earth System Sciences*, *13*(1), 69–77.
Kassambara, A., & Mundt, F. (2017). factoextra: Extract and visualize the results of multivariate data analyses. Computer software manual.
Lewandowski, J., Arnon, S., Banks, E., Batelaan, O., Betterle, A., Broecker, T., et al. (2019). Is the hyporheic zone relevant beyond the scientific community? *Water*, *11*(11), 2230.
Lewandowski, J., Lischeid, G., & Nützmann, G. (2009). Drivers of water level fluctuations and hydrological exchange between groundwater and surface water at the lowland River Spree (Germany): Field study and statistical analyses. *Hydrological Processes*, *23*(15), 2117–2128.
Ling, J., & Dybbs, A. (1992). The effect of variable viscosity on forced convection over a flat plate submersed in a porous medium. *Journal of Heat Transfer*, *114*(4), 1063–1065.
Malzone, J. M., Anseeuw, S. K., Lowry, C. S., & Allen-King, R. (2016). Temporal hyporheic zone response to water table fluctuations. *Groundwater*, *54*(2), 274–285.
Marzadri, A., Tonina, D., & Bellin, A. (2013). Effects of stream morphodynamics on hyporheic zone thermal regime. *Water Resources Research*, *49*, 2287–2302. https://doi.org/10.1002/wrcr.20199

Marzadri, A., Tonina, D., Bellin, A., & Valli, A. (2016). Mixing interfaces, fluxes, residence times and redox conditions of the hyporheic zones induced by dune-like bedforms and ambient groundwater flow. *Advances in Water Resources*, *88*, 139–151.
Millington, R. J., & Quirk, J. P. (1961). Permeability of porous solids. *Transactions of the Faraday Society*, *57*(0), 1200–1207. https://doi.org/10.1039/TF9615701200
Nield, D. A., & Bejan, A. (2013). *Convection in porous media*. New York, NY: Springer New York. https://doi.org/10.1007/978-1-4614-5541-7
Olden, J. D., & Naiman, R. J. (2010). Incorporating thermal regimes into environmental flows assessments: Modifying dam operations to restore freshwater ecosystem integrity. *Freshwater Biology*, *55*(1), 86–107.
Pedretti, D., Russian, A., Sanchez-Vila, X., & Dentz, M. (2016). Scale dependence of the hydraulic properties of a fractured aquifer estimated using transfer functions. *Water Resources Research*, *52*, 5008–5024. https://doi.org/10.1002/2016WR018660
Poole, G. C., & Berman, C. H. (2001). An ecological perspective on in-stream temperature: Natural heat dynamics and mechanisms of human-causedthermal degradation. *Environmental Management*, *27*(6), 787–802.
R Core Team (2014). R: A language and environment for statistical computing, R Foundation for Statistical Computing. Computer software manual). Vienna, Austria. Retrieved from http://www.R-project.org/
Ramirez, N., & Saez, A. E. (1990). The effect of variable viscosity on boundary-layer heat transfer in a porous medium. *International Communications in Heat and Mass Transfer*, *17*(4), 477–488.
Rau, G. C., Andersen, M. S., McCallum, A. M., Roshan, H., & Acworth, R. I. (2014). Heat as a tracer to quantify water flow in near-surface sediments. *Earth-Science Reviews*, *129*, 40–58. https://doi.org/10.1016/j.earscirev.2013.10.015
Rousseeuw, P. J. (1987). Silhouettes: A graphical aid to the interpretation and validation of cluster analysis. *Journal of Computational and Applied Mathematics*, *20*, 53–65.
Sawyer, A. H., Bayani Cardenas, M., Bomar, A., & Mackey, M. (2009). Impact of dam operations on hyporheic exchange in the riparian zone of a regulated river. *Hydrological Processes: An International Journal*, *23*(15), 2129–2137.
Sawyer, A. H., Bayani Cardenas, M., & Buttles, J. (2012). Hyporheic temperature dynamics and heat exchange near channel-spanning logs. *Water Resources Research*, *48*, W01529. https://doi.org/10.1029/2011WR011200
Sawyer, A. H., & Cardenas, M. B. (2009). Hyporheic flow and residence time distributions in heterogeneous cross-bedded sediment. *Water Resources Research*, *45*, W08406. https://doi.org/10.1029/2008WR007632
Schmadel, N. M., Ward, A. S., Lowry, C. S., & Malzone, J. M. (2016). Hyporheic exchange controlled by dynamic hydrologic boundary conditions. *Geophysical Research Letters*, *43*, 4408–4417. https://doi.org/10.1002/2016GL068286
Schuite, J., Flipo, N., Massei, N., Rivière, A, & Baratelli, F. (2019). Improving the spectral analysis of hydrological signals to efficiently constrain watershed properties. *Water Resources Research*, *55*, 4043–4065. https://doi.org/10.1029/2018WR024579
Singh, T., Wu, L., Gomez-Velez, J. D., Lewandowski, J., Hannah, D. M., & Krause, S. (2019). Dynamic hyporheic zones: Exploring the role of peak flow events on bedform-induced hyporheic exchange. *Water Resources Research*, *55*, 218–235. https://doi.org/10.1029/2018WR022993
Song, X., Chen, X., Stegen, J., Hammond, G., Song, H.-S., Dai, H., et al. (2018). Drought conditions maximize the impact of high-frequency flow variations on thermal regimes and biogeochemical function in the hyporheic zone. *Water Resources Research*, *54*, 7361–7382. https://doi.org/10.1029/2018WR022586
Stoica, P., & Moses, R. L. (1997). *Introduction to spectral analysis* (Vol. 1). Upper Saddle River, NJ: Prentice Hall.
Stonedahl, S. H., Harvey, J. W., Wörman, A., Salehin, M., & Packman, A. I. (2010). A multiscale model for integrating hyporheic exchange from ripples to meanders. *Water Resources Research*, *46*, W12539. https://doi.org/10.1029/2009WR008865
Todd, D. K., & Mays, L. W. (2005). Groundwater hydrology edition. Welly Inte.
Tonina, D., & Buffington, J. M. (2011). Effects of stream discharge, alluvial depth and bar amplitude on hyporheic flow in pool-riffle channels. *Water Resources Research*, *47*, W08508. https://doi.org/10.1029/2010WR009140
Trauth, N., & Fleckenstein, J. H. (2017). Single discharge events increase reactive efficiency of the hyporheic zone. *Water Resources Research*, *53*, 779–798. https://doi.org/10.1002/2016WR019488
Trauth, N., Schmidt, C., Maier, U., Vieweg, M., & Fleckenstein, J. H. (2013). Coupled 3-D stream flow and hyporheic flow model under varying stream and ambient groundwater flow conditions in a pool-riffle system. *Water Resources Research*, *49*, 5834–5850. https://doi.org/10.1002/wrcr.20442
Wörman, A., Packman, A. I., Marklund, L., Harvey, J. W., & Stone, S. H. (2006). Exact three-dimensional spectral solution to surface-groundwater interactions with arbitrary surface topography. *Geophysical Research Letters*, *33*, L07402. https://doi.org/10.1029/2006GL025747
Wörman, A., Riml, J., Schmadel, N., Neilson, B. T., Bottacin-Busolin, A., & Heavilin, J. (2012). Spectral scaling of heat fluxes in streambed sediments. *Geophysical Research Letters*, *39*, L23402. https://doi.org/10.1029/2012GL053922
Ward, J. V. (1985). Thermal characteristics of running waters. In *Perspectives in Southern Hemisphere limnology* (pp. 31–46). Dordrecht: Springer.
Ward, A. S., Schmadel, N. M., Wondzell, S. M., Gooseff, M. N., & Singha, K. (2017). Dynamic hyporheic and riparian flow path geometry through base flow recession in two headwater mountain stream corridors. *Water Resources Research*, *53*, 3988–4003. https://doi.org/10.1002/2016WR019875
Weiskel, P. K., Brandt, S. L., DeSimone, L. A., Ostiguy, L. J., & Archfield, S. A. (2010). Indicators of streamflow alteration, habitat fragmentation, impervious cover, and water quality for Massachusetts stream basins. (Ver 1.8, 2 July, 2013), U.S. Geological Survey Scientific Investigations Report 2009–5272, (70 pp.). Retrieved from http://pubs.usgs.gov/sir/2009/5272/
Woodside, W., & Messmer, J. H. (1961). Thermal conductivity of porous media. I. Unconsolidated sands. *Journal of Applied Physics*, *32*(9), 1688–1699. https://doi.org/10.1063/1.1728419
Wu, L., Singh, T., Gomez-Velez, J., Nützmann, G., Wörman, A., Krause, S., & Lewandowski, J. (2018). Impact of dynamically changing discharge on hyporheic exchange processes under gaining and losing groundwater conditions. *Water Resources Research*, *54*, 10,076–10,093. https://doi.org/10.1029/2018WR023185
Zhang, Y.-K., & Schilling, K. (2004). Temporal scaling of hydraulic head and river base flow and its implication for groundwater recharge. *Water Resources Research*, *40*, W03504. https://doi.org/10.1029/2003WR002094
Zheng, L., & Cardenas, M. B (2018). Diel stream temperature effects on nitrogen cycling in hyporheic zones. *Journal of Geophysical Research: Biogeosciences*, *123*, 2743–2760. https://doi.org/10.1029/2018JG004412
Zheng, L., Cardenas, M. B., & Wang, L. (2016). Temperature effects on nitrogen cycling and nitrate removal-production efficiency in bed form-induced hyporheic zones. *Journal of Geophysical Research: Biogeosciences*, *121*, 1086–1103. https://doi.org/10.1002/2015JG003162
Zmijewski, N., & Wörman, A. (2016). Hydrograph variances over different timescales in hydropower production networks. *Water Resources Research*, *52*, 5829–5846. https://doi.org/10.1002/2015WR017775